Finite Element Analysis of Hydro-mechanical Coupling Effects on Shear Failures of Fully Saturated Collapsible Geomaterials

Qiushi Chen[1], M. ASCE, and WaiChing Sun[2], M. ASCE, and Jakob T. Ostien[3]

[1]Department of Civil Engineering, Clemson University, Clemson, SC 29634; qiushi@clemson.edu
[2]Department of Civil Engineering and Engineering Mechanics, Columbia University, New York, NY10027; wsun@columbia.edu
[3]Mechanics of Materials Department, Sandia National Laboratories, Livermore, CA 94551

ABSTRACT: The fully coupled diffusion-deformation processes occurring within porous geomaterials, such as sand, clay and rock, are of interest to numerous geotechnical engineering applications. In this work, a stabilized enhanced strain finite element procedure for poromechanics is integrated with an elasto-plastic cap model to simulate the associative and non-associative hydro-mechanical responses of fluid-infiltrating biphasic collapsible porous geomaterials. We present a quantitative analysis on how macroscopic plastic response caused by pore collapse and grain rearrangement affects the seepage of pore fluid, and vice versa. Finite element simulations of shear failure problems will be presented to study the effect of pore pressure dissipation on the stress path and plastic response of the porous geomaterials.

INTRODUCTION

The fully coupled diffusion-deformation processes occurring within porous media, such as sand, clay, and rock, are of interest to numerous geotechnical engineering applications. The presence of fluid inside the pores and in between the interconnected grains may induce excess pore pressure, limit volumetric deformation, and introduce rate dependence to the mechanical response of the solid skeleton due to the transient nature of fluid diffusion (Coussy 2004; Rice and Cleary 1976). Since pore-fluid flow may profoundly change the mechanical response of porous media, it is important to take it into account to ensure the sufficiency of engineering designs.

The fluid-solid interaction in porous media is often viewed in the context of mixture theory, in which one or multiple fluids in the connected pore network and a solid skeleton are homogenized as constituents of a continuum mixture (Biot 1941; Coussy 2004). The resulting boundary value problem leads to a two-way coupled system involving at least two sets of balance equations: one to characterize the deformation of the solid skeleton, and one for the mass balance of the pore fluid.

There is an extensive body of literature focusing on finite element analysis of such a coupled system for geotechnical engineering applications (Jeremic et al. 2008; Prevost 1982; Sun et al. 2013b). Some of these efforts incorporate critical state plasticity models to capture shear failure and strain localization underneath the foundation. This type of shear failure may be accompanied by various amounts of plastic dilation. Nevertheless, geomaterials, such as high-porosity rock and salt, are vulnerable to both shear and compaction failure. To capture the inelastic compactive behavior of fully saturated rock, we incorporate a cap plasticity model that uses a pressure-dependent shear yielding/failure surface with a hardening compactive elliptical cap to capture the pore collapse (Foster et al. 2005; Regueiro and Foster 2011). This model features a material state that may move freely from compactive to shear-dominated dilative deformation. The third stress invariant is introduced to capture the difference in strength of geomaterials observed in triaxial compression and extension tests.

Another upshot of the current formulation is the introduction of stabilization procedure to enable the usage of the same finite element space for both displacement and pore pressure (Sun et al. 2013b; White and Borja 2008) and the usage of a new combined F-bar method to avoid volumetric locking (Sun et al. 2013a; Sun et al. 2013b). The formulation is then integrated with a cap-surface model to simulate the fully coupled deformation-diffusion process exhibited in porous rock, which are often encountered in energy-related applications. By integrating the cap-surface model with the stabilized hydro-mechanical scheme, we study how inelastic compaction affects the hydraulic response of collapsible porous media and predict whether the presence of pore-fluid would delay or promote inelastic compaction.

ASSUMED STRAIN MIXED FINITE ELEMENT FORMULATION

In this section, a stabilized assumed strain mixed finite element formulation for solving poromechanics problem is briefly summarized. The central premise of the poromechanics theory is that the total stress, $\boldsymbol{\sigma}$, experienced by the solid-fluid mixture is the sum of effective stress $\boldsymbol{\sigma}'$ experienced by the solid skeleton and the pore pressure p induced by the pore fluid i.e.,

$$\boldsymbol{\sigma} = \boldsymbol{\sigma}' - Bp\boldsymbol{I} \tag{1}$$

where $B = 1 - K/K_s$ is the Biot's coefficient, a scalar parameter related to the solid skeleton bulk modulus K and the solid grain bulk modulus K_s, and $\boldsymbol{I}$ is the second order identity tensor.

The governing equations for mixed finite element formulation consist of balance of linear momentum and balance of mass, which are given as

$$\nabla^x \cdot (\boldsymbol{\sigma}' - Bp\boldsymbol{I}) + \boldsymbol{\gamma} = \boldsymbol{0} \tag{2}$$

$$-B\nabla^x \cdot \dot{\boldsymbol{u}} - \frac{1}{M}\dot{p} + \nabla^x \cdot \frac{1}{\mu}\boldsymbol{k}(\nabla^x p + \gamma^f) = 0 \tag{3}$$

where $\boldsymbol{\gamma} = \boldsymbol{\gamma}^s + \boldsymbol{\gamma}^f$ is the total unit weight consisting of solid (superscript 's') and fluid (superscript 'f') part. $\boldsymbol{u}$ is solid displacement vector, the superimposed dot is for

time derivative. M is the Biot modulus, and k is the intrinsic permeability of the porous system. For Biot modulus M, the following form proposed in (Biot 1941; Coussy 2004) are used.

$$M = \frac{K_s K_f}{K_f (B - \phi^f) + K_s \phi^f} \tag{4}$$

where K_s and K_f are the bulk moduli of the solid grain nd the pore-fluid constituents. The weak form of the poromechanics problem is then obtained by coupling Eqs. (2) and (3) and applying the principle of virtual work. To maintain stability, we project the interpolated pore pressure field onto a constant and introduce it in the weak form of (3) to maintain numerical stability. On the other hand, the volumetric locking of the numerical solution is circumvented by an assumed strain method. In particular, an assumed strain method which derives directly from the assumed deformation gradient method in (Sun et al. 2013b) is utilized. The central idea is to replace the standard infinitesimal strain field with an incompatible assumed strain field $\bar{\boldsymbol{\varepsilon}}$

$$\bar{\boldsymbol{\varepsilon}} = \frac{1}{2}(\boldsymbol{F} + \bar{\boldsymbol{F}} - 2\boldsymbol{I}) \tag{5}$$

where $\bar{\boldsymbol{F}}$ is the assumed deformation gradient that overcomes the volumetric locking. Interested readers may referred to (Sun et al. 2013a and Sun et al. 2013b) for detail.

CAP PLASTICITY MODEL AND NUMERICAL IMPLEMENTATION

Cap models are typically used in the modeling of complicated behavior of porous geomaterials. The formulation and numerical implementation of a three-invariant, isotropic and kinematic hardening cap plasticity model are briefly presented in this section. The model is composed of pressure-dependent shear yield surface and a hardening compaction cap as shown in Fig. 1.
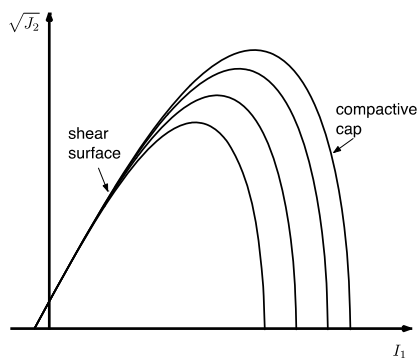

Fig. 1. Cap plasticity model yield surface.

Model formulation

Before introducing the yield and plastic potential functions, a deviatoric back stress tensor $\boldsymbol{\alpha}$ is presented to capture the Bauschinger effect, such that the relative stress tensor can be defined as $\boldsymbol{\xi} = \boldsymbol{\sigma} - \boldsymbol{\alpha}$. The three stress invariants of the relative

stress tensor are $I_1 = \sigma_{ii}$, $J_2^\xi = \frac{1}{2}\boldsymbol{\xi}:\boldsymbol{\xi}$, and $J_3^\xi = \frac{1}{3}(\xi)$. The superscript ξ means the quantity is expressed in term of relative stress tensor $\boldsymbol{\xi}$. The yield surface f and plastic potential function g of the cap model are both written in terms of stress invariants of relative stress tensor, i.e., I_1, J_2^ξ, J_3^ξ, as

$$f = (\Gamma(\beta^\xi))^2 J_2^\xi - F_c(F_f - N)^2 = 0 \tag{6}$$

$$g = (\Gamma(\beta^\xi))^2 J_2^\xi - F_c^g(F_f^g - N)^2 \tag{7}$$

where F_f is an exponential shear failure function, and F_f^g is the corresponding plastic potential surface given as

$$F_f = A - C\exp(DI_1) - \theta I_1 \tag{8}$$
$$F_f^g = A - C\exp(LI_1) - \phi I_1 \tag{9}$$

The shear failure surface F_f captures the pressure-dependence of the shear strength of the material. N is a material parameter that represents the offset of the yield function from shear failure surface. A, C, D and θ are material parameters fit to experimental peak stress. L and ϕ are determined from experimental measurements of volumetric plastic deformation. $\Gamma(\beta_\xi)$ is a function of the Lode angle β, which is given as

$$\Gamma(\beta^\xi) = \frac{1}{2}\left(1 + \sin(3\beta^\xi) + \frac{1}{\varphi}(1 - \sin(3\beta^\xi))\right) \tag{10}$$

where φ is the ratio of triaxial extension strength to compression strength. F_c provides a smooth elliptical cap to the yield function and is given as

$$F_c = 1 - H(\kappa - I_1)\left(\frac{I_1 - \kappa}{X(\kappa) - \kappa}\right)^2 \tag{11}$$

where $H(\kappa - I_1)$ is the Heaviside function. The function $X(\kappa)$ is the intersection of the cap surface with the I_1 axis in the meridional stress space, and is given as

$$X(\kappa) = \kappa - RF_f(\kappa) \tag{12}$$

where R is a material parameter governing the aspect ratio of the cap surface. The corresponding functions for the plastic potential g are given as

$$F_c^g = 1 - H(\kappa - I_1)\left(\frac{I_1 - \kappa}{X^g(\kappa) - \kappa}\right)^2 \tag{13}$$

$$X^g(\kappa) = \kappa - QF_f(\kappa) \tag{14}$$

where Q is a material parameter analogous to R.

There are two internal variables involved in the cap plasticity model: the cap hardening parameter κ for isotropic hardening, and the back stress $\boldsymbol{\alpha}$ for kinematic hardening. The evolution of κ is related to the volumetric plastic strain while the evolution of $\boldsymbol{\alpha}$ is related to the deviatoric plastic strain. The evolution expressions are given as

$$\dot{\boldsymbol{\alpha}} = \dot{\gamma}\boldsymbol{h}^\alpha(\boldsymbol{\alpha}) \tag{15}$$

$$h^{\alpha} = c^{\alpha} G^{\alpha}(\boldsymbol{\alpha}) \text{dev}\left(\frac{\partial g}{\partial \boldsymbol{\sigma}}\right) \tag{16}$$

where $\dot{\gamma}$ is the consistency parameter, and c^{α} is a material parameter that controls the rate of hardening. $G^{\alpha}(\boldsymbol{\alpha}) = 1 - \dfrac{\boldsymbol{\alpha}:\boldsymbol{\alpha}}{2N}$ is a function which limits the growth of the backstress as it approaches the failure surface.

The evolution of isotropic hardening parameter κ, is given as

$$\dot{\kappa} = \dot{\gamma} \boldsymbol{h}^{\kappa}(\kappa) \tag{17}$$

$$h^{\kappa} = \frac{tr\left(\frac{\partial g}{\partial \boldsymbol{\sigma}}\right)}{\frac{\partial \varepsilon_v^p}{\partial \kappa}} \tag{18}$$

where ε_v^p is the volumetric plastic strain, which is computed from

$$\varepsilon_v^p = W\{\exp[D_1(X(\kappa) - X_0) - D_2(X(\kappa) - X_0)^2] - 1\} \tag{19}$$

In the above, W, D_1 and D_2 are material parameters, $X_0 = X(\kappa_0)$ is the initial cap position with κ_0 being the initial value of the cap parameter, a material constant.

Numerical implementation

Given the values of stress and internal variables at time t_n, and the strain increment $\Delta\boldsymbol{\varepsilon}$, the goal of the numerical integration is to find the stress and internal variable values at time t_{n+1}. This is accomplished using the evolution equations (15), (17) while at the same time satisfy the yield condition (6). In this work, we employ both implicit and a refined explicit integration algorithms, which contains an automatic stress correction algorithm (Slone et al., 2001) to prevent stress and hardening parameters from drifting away from the yield surface. Alternatively, a semi-implicit algorithm proposed by (Tu et al. 2009) for integrating non-smooth elasto-plastic models may be applied.

The proposed assumed strain coupled finite element formulation and the cap plasticity model are integrated within Sandia National Laboratories' ALBANY analysis code (Salinger et al. 2013). The code is designed for the rapid development of finite-element analysis capabilities enabled through the concept of agile components, where generic building blocks of capabilities are readily assembled to meet the requirements of ultimate analysis application. Genericism is provided by the use of template-based generic programming (TBGP) techniques. The code's components are implemented to operate on general template data types, which specialized at, compile time to deliver the desired capabilities. As an outcome of this overall design, ALBANY has a unique infrastructure that limits the need for programming to just writing the physics residual equations based on a generic type; ALBANY will then compute the system Jacobian and pre-conditioner for the Newton nonlinear solver. ALBANY is openly available at the download sites given in the bibliography.

NUMERICAL EXAMPLES

In this section, we present finite element analysis of an unconfined drained shear failure problem. The objectives are two-folds: (i) to analyze how local pore-fluid diffusion may affect the formation of a shear band; and (ii) to provide a numerical assessment of the rate effect induced by the seepage on the mechanical responses. We assume isotropic homogeneous media and isotropic permeability tensor. The analysis is performed in small-deformation region. The boundary conditions are illustrated in

Fig. 2. Gravity is neglected. All material properties are calibrated to Salem limestone data, as reported in (Sun et al. 2013a) and reference therein. It should be also pointed out that if field data is available, it would be desirable to present the load with respect to initial in situ stress. But in current work, we assume zero initial stress.
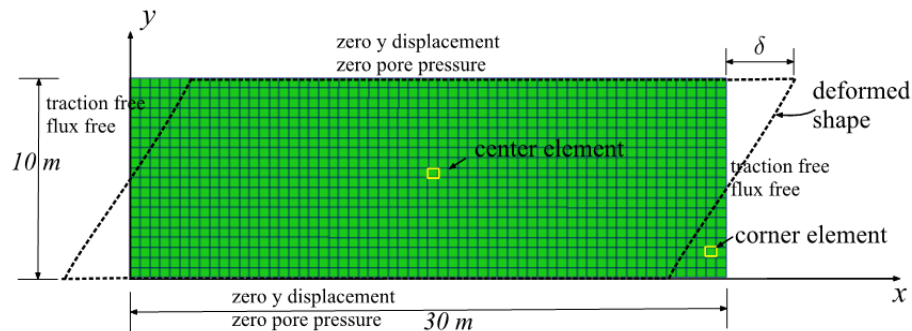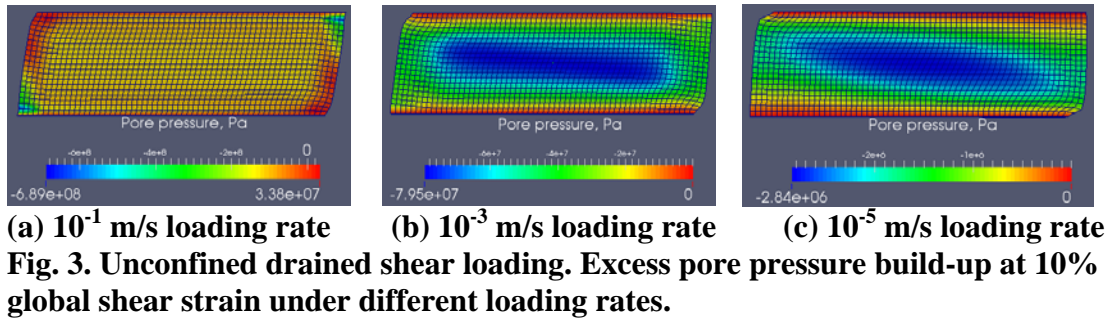

Fig. 2. Boundary conditions of the unconfined drained shear loading. Highlighted elements are for reporting stress paths.

Rate effects

First, we assess the importance of rate effects on local excess pore pressure build-up and analyze whether the non-uniformity of excess pore pressure causes significant effects on the mechanical response. For comparison, we prescribed the horizontal displacement of the top and bottom of the specimens at three different loading rates: 10^{-1}, 10^{-3}, and 10^{-5} m/second. This difference in prescribed loading rates leads to various amounts of shear-induced diffusion and pore pressure build-up. Fig. 3 demonstrates the amount excess pore pressure generated when the prescribed shear strain reaches 10%.

(a) 10^{-1} m/s loading rate   **(b) 10^{-3} m/s loading rate**   **(c) 10^{-5} m/s loading rate**
Fig. 3. Unconfined drained shear loading. Excess pore pressure build-up at 10% global shear strain under different loading rates.

All the simulations are globally drained. In an idealized situation where local seepage is neglected, all simulations are expected to yield the same result. However, the results presented in this example clearly indicate that the local pore-fluid diffusion may introduce discrepancies in mechanical response if the ratio between loading rate and hydraulic conductivity is sufficiently high. In addition, the local pore pressure build-up during the shear phase influence the effective stress path and elaso-plastic responses. Fig. 4 compares the equivalent plastic strain developed at various loading rates in fully saturated and dry simulations. For illustration purposes, quantities such as equivalent plastic strains at integration points are projected onto the nodes via a global L_2 projection scheme (Mota et al. 2013).

(a) dry case   **(b) 10^{-5} m/s loading rate**
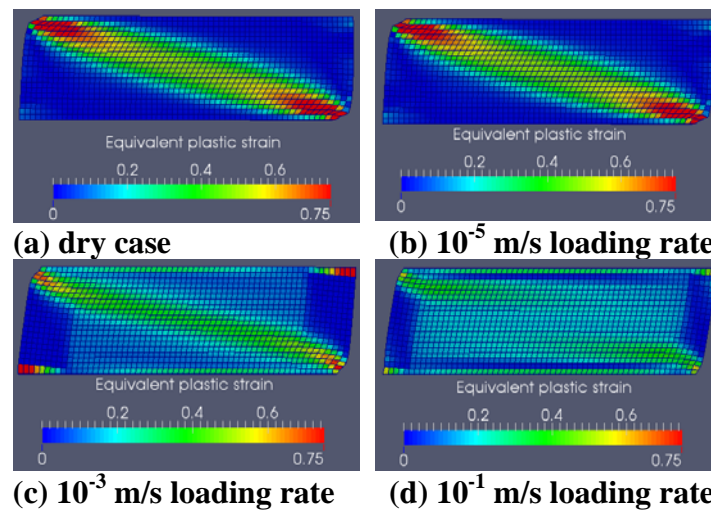**(c) 10^{-3} m/s loading rate**   **(d) 10^{-1} m/s loading rate**
Fig. 4. Unconfined drained shear loading. Equivalent plastic strain contours at 10% global shear strain for dry simulation and poro-mechanical coupling simulations under different loading rates.

By comparing the plastic responses shown in Fig. 4, it is observed that two-way, hydro-mechanical coupling effect is more substantial when the prescribed loading rate is high. For instance, the equivalent plastic strain of the dry case and the coupled simulation with a 10^{-5} m/second loading rate are similar to each other. While a localized shear band still forms in the 10^{-3} m/second loading rate case, the specimen exhibits less equivalent plastic strain in the shear band zone, as shown in Fig. 4 (c). When loading rate reaches 10^{-1} m/second, the hydro-mechanical coupling effect is found to be sufficient to prevent the formation of shear band, as shown in Fig. 4 (d).

In the fastest loading rate case, 10^{-1} m/second, the pore fluid trapped at the middle of the specimen causes a significant pore pressure that prevents the formation of the shear band. More importantly, it clearly shows that fully saturated porous media under drained conditions may behave very differently than the dry solid skeleton if the loading rate is high.

As demonstrated by the non-uniform plastic response in Fig. 4, local stress paths at different locations differ significantly. To this end, the relative stress paths obtained from the center and the right bottom corner of the specimen at various loading rates (locations of selected elements highlighted in

Fig. 2) are reported in. At both locations, the effective stress response of the slowest loading rate (10^{-5} m/second) and the dry case coincide with each other. This similarity in stress path, and the small pore pressure are shown in Fig. 3 indicate that the hydro-mechanical coupling effect is weak at a slow loading rate. However, when the loading rate increases, more negative pore pressure is accumulated and thus pushes the specimen closer to the undrained limit, which ultimately leads to higher effective hydrostatic and deviatoric stress in the center of the specimen.

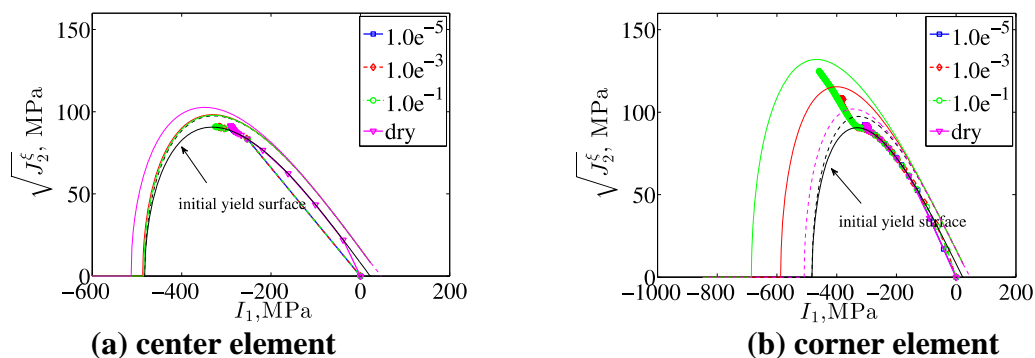**(a) center element**   **(b) corner element**

Fig. 5. Unconfined drained shear loading. Relative stress path in meridional stress space for structured fine mesh. The solid lines are the final yield surfaces, colored to match different loading rates.

Mesh Sensitivity

The fully coupled hydro-mechanical response is rate dependent due to the diffusion of pore fluid. This rate dependence might provide regularization on the numerical solutions as discussed previously in (Belytschko et al. 2000). Detailed studies by Zhang and Schrefler (2001) on dynamics of porous media reveals that the presence of pore fluid may alter the onset of bifurcation condition, and introduce length scale that strongly depends on permeability.

Fig. 6 compares the equivalent plastic strain accumulated from two uniform meshes. We observe that the plastic response of the shear band is sensitive to mesh refinement in the dry case, as shown Fig. 6 (b) and (d). In particular the plastic zone of the finite mesh accumulates significantly more equivalent plastic strain than the coarse mesh counterpart. While a similar discrepancy can still be observed in the fully saturated specimen, the difference on equivalent plastic strain is much smaller. To accurately analyze how pore-fluid diffusion affects the onset of strain localization, algorithms that detect a singularity in the acoustic tensor are required. This topic will be considered in future studies.

(a) fully saturated   **(b) dry specimen**

(c) fully saturated   **(d) dry specimen**
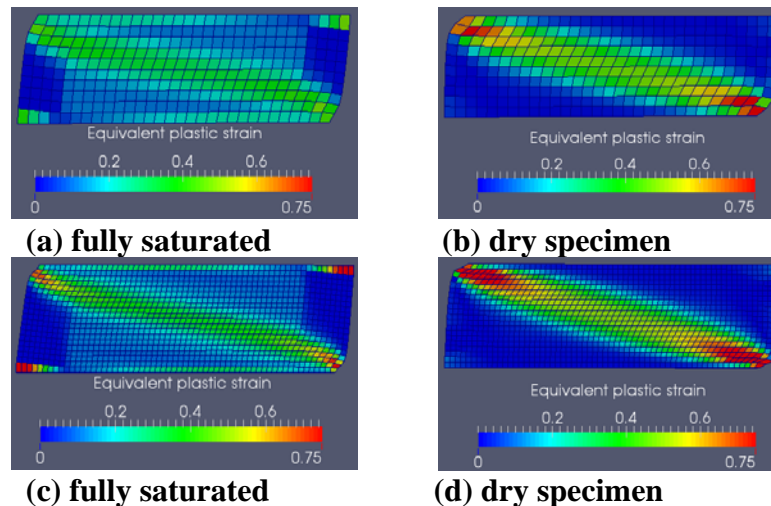
Fig. 6. Unconfined drained shear loading. Equivalent plastic strain contours of fully saturated (left) and dry (right) specimens obtained from coarse and fine structured meshes at 10% global shear strain.

CONCLUSIONS

In this work, we examine the fully coupled hydro-mechanical response of water-saturated limestone subjected to shear loadings with various rates. The cap-plasticity model is incorporated into a stabilized mixed finite element method to simulate the fully coupled deformation-diffusion process of collapsible porous media. We found that hydro-mechanical couplings may impose various degrees of influence on the mechanical responses, depending on the loading rate and geometry of the domain. In the case of shear failure of saturated porous medium, the local pore-fluid may prevent the formation of shear band.

ACKNOWLEDGEMENTS

REFERENCES

Biot, M.A. (1941). "General theory of three dimensional consolidation." *Journal of Applied Physics,* 12(2), 155 –164.

Coussy, O. (2004). *Poromehcanics.* Wiley, New York.

Foster, C.D., Regueiro, R.A., Fossum, A.F., and R. I. Borja, R.I. (2005). "Implicit numerical integration of a three-invariant, isotropic/kinematic hardening cap plasticity model for geomaterials." *Computer Methods in Applied Mechanics and Engineering,* 194, 5109–5138.

Jeremic, B., Cheng, Z., Taiebat, M., and Dafalias, Y. (2008). "Numerical simulation of fully saturated porous materials." *International Journal for Numerical and Analytical Methods in Geomechanics,* 32, 1635–1660.

Mota, A., Sun, W., Ostien, J.T., Foulk, J.W., and Long, K.N. (2013). "Lie-group interpolation and variational recovery for internal variables." *Computational Mechanics,* 52, 1281-1299.

Prevost, J.H. (1982). "Nonlinear transient phenomena in saturated porous media." *Computer Methods in Applied Mechanics and Engineering,* 30(1), 3-18,.

Regueiro, R.A. and Foster, C.D. (2011). "Bifurcation analysis for a rate-sensitive, non-associative, three-invariant, isotropic/kinematic hardening cap plasticity model for geomaterials: Part i. small strain." *International Journal for Numerical and Analytical Methods in Geomechanics,* 35, 201–225.

Rice, J.R. and Cleary, M.P. (1976). "Some basic stress diffusion solutions for fluid-saturated elastic porous media with compressible constituents." *Rev. Geophys.,* 14(2), 227–241.

Salinger et al. (2013). "Albany: A Component-based partial differential equation code built on Trilinos." *ACM Transaction on Mathematical Software*, in review.

Sloan, S., Abbo, A. and Sheng, D. (2001). "Refined explicit integration of elastoplastic models with automatic error control." *Engineering Computations,* 18, 121–154.

Sun, W., Chen, Q. and Ostien, J.T. (2013a). "Modeling the hydro-mechanical responses of strip and circular punch loadings on water-saturated collapsible geomaterials" *International Acta Geotechnica,* in press.

Sun, W., Ostien, J.T., and Salinger, A. (2013b). "A stabilized assumed deformation gradient finite element formulation for strongly coupled poromechanical simulations at finite strain." *International Journal for Numerical and Analytical Methods in Geomechanics*, 37(16), 2755-2788.

Tu, X., Andrade, J.E., and Chen, Q. (2009). "Return mapping for nonsmooth and multiscale elastoplasticity." *Computer Methods in Applied Mechanics and Engineering,* 198, 2286 – 2296.

White, J.A. and Borja, R.I. (2008). "Stabilized low-order finite elements for coupled solid-deformation/fluid-diffusion and their application to fault zone transients." *Computer Methods in Applied Mechanics and Engineering,* 197(49), 4353–4366.

Zhang, H.W. and Schrefler, B.A. (2001). "Uniqueness and localization analysis of elastic plastic saturated porous media." *International Journal for Numerical and Analytical Methods in Geomechanics,* 25(1), 29–48.